Physica C: Superconductivity and its applications 626 (2024) 1354588

Contents lists available at ScienceDirect

Physica C: Superconductivity and its applications

journal homepage: www.elsevier.com/locate/physc

Full Length Article

Electro-thermal dynamics in superconducting generators: An In-Depth investigation of AC losses and cooling techniques for a 10 MW rotor coil system

A. Erciyas [a], Ş. Yildiz [b,*], F. Inanir [c]

[a] Department of Electricity and Energy, Vocational School of Technical Sciences, Amasya University, Amasya, Turkey
[b] Department of Metallurgical and Materials Engineering, Faculty of Engineering and Architecture, Kırşehir Ahi Evran University, Kırsehir, Turkey
[c] Department of Physics, Yildiz Techical University, 3440 Esenler/Istanbul, Turkey

ARTICLE INFO

Keywords:
Superconducting generators
AC Loss
Cooling of Coil system

ABSTRACT

In the pursuit of optimizing superconducting generator systems, a comprehensive understanding of their electro-thermal behaviors is crucial. This study builds upon previous research on an 8-pole, 10 MW superconducting generator by Inanir et al. (2022, Journal of Superconductivity and Novel Magnetism, 35(11), 3189) and focuses on an in-depth electro-thermal analysis of the rotor coil system. The emphasis is on assessing the AC losses experienced during transitory current changes. By simultaneously solving Ampere's equation and the heat conduction equation under specific boundary conditions, the research provides a detailed insight into the interaction between electrical and thermal dynamics within the rotor coils. The paper highlights the importance of temperature dynamics in various cooling and current conditions. The results demonstrate that achieving an optimal balance in cooling, particularly with the use of liquid nitrogen, is critical for efficient operation. This study not only advances the understanding of superconducting generators but also highlights potential strategies for improving their reliability and efficiency.

1. Introduction

Superconducting generators hold great promise for reducing energy losses and improving system efficiency, especially as the world's energy demands rise. Even though large offshore projects have already developed and implemented 15 MW class wind turbine generators utilizing machinery made up of normal conductors, such as the Vestas V236-15.0 MW [1], superconducting generators still provide a number of advantages that warrant further study and engineering [2]. These advantages encompass enhanced efficiency and reduced weight, which are vital for next-generation energy solutions. This work focuses on comprehending the electro-thermal dynamics of the rotor system of a superconducting generator, particularly under current variations, in order to overcome the technological challenges and fully utilize these advantages.

Several studies have delved into the nuances of superconducting generators, exploring their design [3-12], loss mechanisms [13-17], and cryogenic cooling requirements [18-22] over the past few decades. For instance, our previous work (Ref. [12]) made significant strides by investigating the design of a 10 MW wind turbine generator and the alternating current (AC) loss analysis for its superconducting rotor coils. Building on that foundation, the present paper intends to delve deeper, focusing on the electro-thermal dynamics, particularly during transitory changes in coil currents.

Historically, AC losses in superconducting tapes have been a focal point of numerous investigations [22-28]. These losses, influenced by magnetic fields, determine the thermal behavior of the system. An imbalance or spike in temperature can potentially lead to quenching – a state where the superconductor loses its zero-resistance property, jeopardizing the entire system's performance. Hence, understanding and controlling these temperature dynamics is critical. However, while AC losses have been extensively studied in isolation, fewer studies have explored them in conjunction with electro-thermal behaviors during current transients in large systems, such as the 10 MW superconducting generator considered in our study. This gap, although seemingly narrow, is significant in practice. It determines the real-world viability of these generators in dynamic grid scenarios where load changes and system transitions are frequent.

Our earlier work, which examined the design and AC loss analysis of

* Corresponding author at: Kırşehir Ahi Evran University.
E-mail address: sukruyldz@gmail.com (Ş. Yildiz).

https://doi.org/10.1016/j.physc.2024.1354588
Received 1 June 2024; Received in revised form 27 August 2024; Accepted 27 August 2024
Available online 29 October 2024

the superconducting rotor coils of a 10 MW wind turbine generator, provided a remarkable contribution in terms of the loss mechanisms in such systems [12]. The present work seeks to expand on that foundation by delving further into the electro-thermal characteristics, particularly during transitory variations in coil currents. The originality of this study lies in its comprehensive integration of insights from various domains to present a detailed analysis of the electro-thermal interactions within superconducting generators.

By addressing the fragmented nature of existing literature on cooling methodologies and expanding on our previous findings, this paper provides a holistic view of the electro-thermal dynamics in superconducting generators. Our approach not only enhances the understanding of these systems but also highlights potential strategies for improving their reliability and efficiency.

2. Modeling

In the realm of superconducting generator systems, understanding the electro-thermal behaviors is pivotal to optimizing and harnessing the full potential of the technology. This section elucidates the foundational modeling aspects implemented for the electro-thermal analysis of a 10 MW superconducting generator's rotor system, highlighting the key methods and assumptions utilized.

The central aspect of our study revolves around the thermal analyses related to AC losses when transitory changes in magnetic field generating direct current (DC) occur within the rotor coils. The crux of these analyses is built upon the electromagnetic insights presented in Ref. [12], which investigated an 8-pole superconducting generator with a steady-state DC current traversing through its field winding. Such systems' efficiency is intrinsically linked with the critical current in the field winding and the AC losses, further influencing the heat these losses produce.

Given the prevalence of a significant self-field or external magnetic field in many superconducting coils, one must consider the limitations placed by the magnetic field's structural anisotropy on the coil's critical current. The heat and AC losses generated by the time increasing and decreasing current loss substantially influence cryogenic designs, and their quantification relies on the distribution of current and magnetic fields. Therefore, the prime focus of this modeling exercise is to accurately estimate the heat produced as the generator rotor's DC current stabilizes, and subsequently devise methodologies to effectively dissipate this heat.

Fig. 1 provides a detailed two-dimensional (2D) cross-sectional visualization of the superconducting racetrack-type "pancake" coil stacks that form a critical part of the rotor system in a 10 MW superconducting generator. The design highlights the strategic placement of the coils in the *xy*-plane, optimized for a current flow predominantly in the *z*-direction. This orientation is essential for the functioning of the generator, as it pertains to the occurrence of AC losses during transitory magnetic field changes that influence the system's thermal dynamics.

The figure depicts each coil as a distinct element within the stack, separated by insulation layers to prevent electrical shorts and to assist in maintaining structural integrity. The spacing between the coils is also indicative of the channels through which liquid nitrogen is circulated, playing a pivotal role in the cooling mechanism. This cryogenic environment is vital for sustaining superconductivity by removing the heat generated due to AC losses, which is directly related to the critical current and the magnetic field's influence on the coils.

The A-V formulation underpins the electromagnetic assessment of the superconducting segment. The principal equations under this framework include [29-32]:

$$\frac{1}{\mu_0\mu_r}(\nabla \times \nabla \times \mathbf{A}) = \mathbf{J} \tag{1}$$

$$J = -\sigma\frac{\partial \mathbf{A}}{\partial t} + J_s \tag{2}$$

where $J_s = -\sigma\nabla\varphi$ represents the coil's source current density and φ is the electric scalar potential. Eq. (3) elucidates the electrical conductivity for superconducting tapes within the A-V formulation, stemming from the non-linear current-voltage interplay [31,32],

$$\sigma = \frac{J_c(B,T)}{E_c}\left(\frac{|E|}{E_c} + \delta\right)^{(1-n)/n} \tag{3}$$

where $J_c(B,T)$ is the field and temperature dependent critical current density, E_c=1 × 10^{-4} V/m is the electric field criterion, and n is the non-

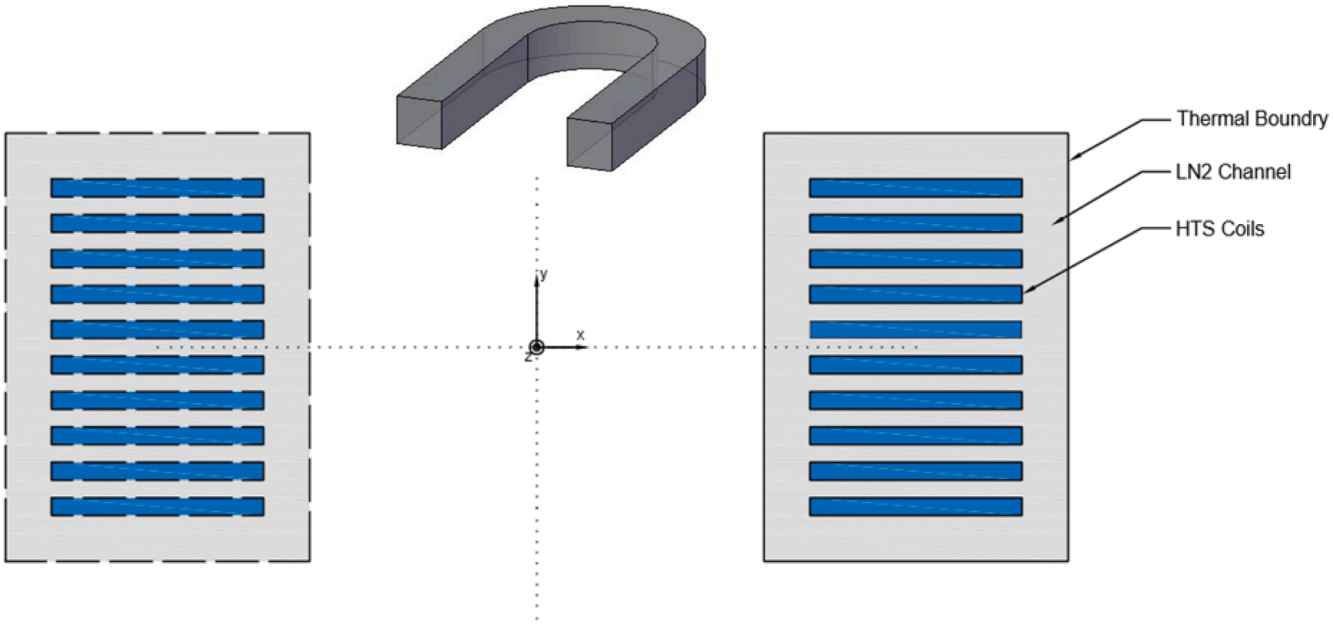

Fig. 1. 2D cross-sectional view of the superconducting racetrack-type pancake coil stacks in a 10 MW generator's rotor system. The illustration represents the coils placed within the *xy*-plane, with current flow oriented in the *z*-direction. The arrangement facilitates cooling through a liquid nitrogen channel flowing in the *xy*-plane, integral to the electro-thermal management of the system.

linear current-voltage exponent. Here, δ=10^{-7} is initially assumed for the $t = 0$ solution, thus avoiding singularity.

The relationship between the electric field (**E**) and the magnetic vector potential (**A**) gets encapsulated as:

$$\mathbf{E} = -\frac{\partial \mathbf{A}}{\partial t} - \nabla\varphi \tag{4}$$

The boundary condition reflecting periodicity of the generator for electromagnetic analysis is provided in Ref. [12].

The thermal behavior over the coil's cross-section is based on

$$C_p(T)\frac{dT}{dt} - \nabla\cdot\left(k_p(T)\nabla T\right) = Q \tag{5}$$

where T is temperature, whereas $k_p(T)$ and $C_p(T)$ are the temperature dependent thermal conductivity and specific heat capacity at constant volume, respectively. The experimentally reported values for these physical parameters [33,34] for Rare-Earth Barium Copper Oxide (ReBCO) materials were adopted in this work. We note that the present study specifically addresses superconducting coils with insulated turns, a distinction that is pertinent given the prevalent use of non-insulated coils in the field. This insulation between turns is a critical factor that influences the thermal and electromagnetic behaviors of the coils, and it is accurately accounted for in our thermal analysis framework. However, the discrete structure of superconducting coils is often sidelined in both electromagnetic and thermal analyses. However, for a precise thermal analysis, it is indispensable to accurately detail the thermal characteristics of the superconducting second generation (2G) ReBCO materials composing the coils. ReBCO tapes consist of a copper substrate, a hastelloy ferromagnetic layer, and a superconducting layer. These properties have been incorporated into the thermal analysis of superconducting coils as described below [35]:

$$\rho_N = \frac{\rho_{Cu}(T)\rho_H(T)(h_{Cu}+h_H)}{\rho_{Cu}(T)h_H + \rho_H h_{Cu}} \tag{6}$$

$$\rho(T) = \frac{\rho_N(T)\rho_{YBCO}(T)(h_N+h_{YBCO})}{\rho_N(T)h_{YBCO} + \rho_{YBCO}h_N} \tag{7}$$

$$C_p(T) = \frac{C_{p,Cu}(T)h_{Cu} + C_{p,H}(T)h_H + C_{p,YBCO}(T)h_{YBCO}}{h_{Cu}+h_H+h_{YBCO}} \tag{8}$$

$$k_p(T) = \frac{k_{p,Cu}(T)h_{Cu} + k_{p,H}(T)h_H + k_{p,YBCO}(T)h_{YBCO}}{h_{Cu}+h_H+h_{YBCO}} \tag{9}$$

where $\rho_{Cu}(T)$ is the temperature-varying resistivity of the oxygen-free high thermal conductivity (OFHC/OF) copper forming the stabilizer of the 2G-coated conducting ReBCO tapes, whereas $\rho_H(T)$ is the temperature-varying resistivity of the Hastelloy FM substrate, and $\rho_{YBCO}(T)$ is the temperature-dependent resistivity of the superconducting layer. The heigths of the copper stabilizer (h_{Cu}), hastelloy layer (h_H), and the superconducting layer (h_{YBCO}) in each tape are taken as 40 μm, 50 μm, and 1 μm, respectively. Thermal conductivity, specific heat values of high-temperature superconductor (HTS), copper, and Hastelloy substrate were extracted from Ref [36].

Instantaneous AC loss due to varying magnetic field and current is obtained by considering the product of the electric field electric field **E** and current density **J**:

$$Q = \int_{t_{min}}^{t_{max}} \left(\int_A \mathbf{J}.\mathbf{E}\, dA \right) dt \tag{10}$$

where t_{min} is the time when the instantaneous current starts to be applied, t_{max} is the time when the current reaches the DC state and dA corresponds to the elementary area of the HTS coil.

The electromagnetic fields surrounding the superconducting strip influence its critical current density. The field dependence is given by [37]:

$$J_c(B) = \frac{J_{c0}}{\left(1 + \frac{\sqrt{B_\perp{}^2 + \alpha^2 B_\parallel{}^2}}{B_0}\right)^\beta} \tag{11}$$

The thermal dependence is represented as [35]:

$$J_c\left(B_x, B_y, T\right) = J_c\left(B_x, B_y\right)\frac{\left(T_c - T\right)^\delta}{\left(T_c - T_{ref}\right)^\delta} \tag{12}$$

Here T_c= 90 K is the critical temperature, T_{ref}=77 K is the temperature at which the coils are operated and δ=1.5 is the temperature exponent. For the thermal boundary condition and coiling, considering the surface cooling via liquid nitrogen [38],

$$-\mathbf{n}\cdot\mathbf{q} = -0.05(T_{Coil} - T_{LN_2}) \tag{13}$$

expression is utilized wherein **n** is the normal of the surface and q is the heat flux. As a thermal isolation boundary condition for the outer envelope through which the fluid channel flows:

$$-\mathbf{n}\cdot\mathbf{q} = 0 \tag{14}$$

In our comprehensive analysis of electro-thermal dynamics within superconducting generators, particularly a 10 MW rotor coil system, we adopted a modified approach using the COMSOL Multiphysics finite-element method (FEM) software with AC/DC and Heat Transfers Modules, leveraging its advanced FEM capabilities. We ventured beyond standard methodologies, opting for an A-V formulation to deeply explore the complexities involved. Our strategy involved a pragmatic assumption of continuous current flow over the superconducting tapes, a departure from considering their discrete nature, to streamline our simulations. As for the meshing technique, a delicately chosen mix of "mapping" for coil stacks and "triangular" for liquid nitrogen regions, was designed to attain a balance between detailed accuracy and computational resources. The overall mesh comprised 148,882 elements, carefully designed to balance detailed accuracy with computational efficiency. We ensured meticulous grid convergence, adhering to stringent tolerances. Crucially, our results underwent a rigorous validation process, benchmarked against the renowned H-Formula, enhancing the credibility of our findings. We ensured grid convergence with stringent tolerance levels, setting a relative tolerance of 1×10^{-8} and an absolute tolerance of 1×10^{-10}. However, we candidly acknowledge the inherent limitations due to our simplified assumptions and chosen meshing approach, which, while efficient, might slightly skew the model's representational depth.

We also made a simplifying assumption by considering the current to flow uniformly over the surface of the ReBCO superconducting tapes, which formed the basis of our coil design. This assumption, while streamlining the analysis, was carefully balanced against the need for accurate representation of the electro-thermal behavior in the superconducting generator's rotor system.

3. Results and discussion

Our research offers a comprehensive analysis of the thermal dynamics within superconducting coil systems, underscored by a focus on pivotal aspects that impact their performance. This encompasses an examination of the efficacy of liquid nitrogen as a cooling agent and its rates of application, which play a vital role in the stability and efficiency of the coils. In addition, we delve into the intricacies of temperature distribution within the system, exploring how spatial and temporal temperature gradients can influence the overall functionality and safety of the system. Our simulations can shed light on these critical factors, offering detailed insights and a deeper understanding of their interplay. Subsequent sections will elucidate these findings, presenting the derived data and its implications for the design and operation of advanced

superconducting applications.

The current increase, denoted as I_{inc}, is represented by the equation $I_{inc}(t) = I_{ap}\left(1 - e^{-t/\tau}\right)$ where I_{ap} represents the value of the applied DC current and τ represents the time constant associated with the rate of current increase. Conversely, the current decrease, denoted as I_{dec}, is expressed by the equation $I_{dec}(t) = I_{ap}e^{-t/\tau}$. These specific current waveforms were selected to simulate the transient conditions that the rotor coil system of a 10 MW superconducting generator might experience during typical operational scenarios, such as startup and shutdown processes. In real-world applications, superconducting generators frequently undergo periods of rapid current changes, and these transients can significantly impact the thermal and electrical performance of the system. By modeling the current increase and decrease using exponential functions, we can closely mimic the dynamic response of the rotor coil to these changes, providing valuable insights into the electrothermal behavior under realistic conditions.

To verify that our numerical analysis method and models give physically correct results, we implemented several validation steps tailored to our unique 10 MW generator cooling strategy. Due to the lack of directly comparable experimental or theoretical evidence in the literature for this particular design, we focused on fundamental physical principles and numerical robustness. We performed a mesh refinement study to ensure solution independence from mesh size and conducted a time step sensitivity analysis to confirm output stability across different time steps. We rigorously checked that our model adhered to conservation principles for energy and charge. A comprehensive sensitivity analysis was carried out, varying key parameters to ensure the model responded as expected to input changes. Additionally, we critically examined our results for physical reasonableness, ensuring they did not violate any known physical laws or constraints. In verification analyses, we adhered to the H-Formulation for superconducting coils, which provides a standardized method for calculating electromagnetic properties in superconducting tapes, thereby ensuring the accuracy of our predictions for critical current densities and magnetic field distributions.

Parameters assumed in the simulations, including those relating to current increase and decrease, are tabulated in Table 1 for reference and clarity in understanding the diverse elements under consideration in the thermal performance of the superconducting coil system. Discussions and interpretations of the simulated results are subsequently presented to facilitate a comprehensive understanding of the thermal behavior and characteristics of the system under varying conditions.

The numerical model of heat transfer phenomena in our study is depicted in Fig. 1, which provides a detailed 2D cross-sectional visualization of the superconducting racetrack-type pancake coil stacks forming a critical part of the rotor system in a 10 MW superconducting generator. The model encompasses various analysis regions, including the superconducting coils, insulation layers, and liquid nitrogen cooling channels. The coils are modeled as racetrack-type pancake coils, consisting of multiple layers of HTS tape. The model includes the thermal properties of the HTS tape, such as the copper substrate, Hastelloy ferromagnetic layer, and superconducting layer (Eqs. (6)-(9)). Insulation layers are placed between the superconducting tapes to prevent electrical shorts and provide structural integrity. These layers also add thermal resistance, influencing the overall heat transfer within the coils. LN_2 channels are incorporated into the model to provide effective cooling. These channels flow through and around the coils, absorbing heat generated within the superconducting material. The heat transfer within the superconducting coils is governed by the heat conduction equation (Eq. (5)). Convective heat transfer boundary conditions are applied to the outer surfaces of the superconducting coils to simulate the cooling effect of liquid nitrogen (Eq. (13)). We employ Eq. (13) As a thermal isolation boundary condition for the outer envelope through which the fluid channel flows.

Table 1
Parameters employed in the calculations.

Quantity (Unit)	Description	Value
I_C (A)	Critical current of HTS tapes	600
w_{SC} (mm)	Width of HTS Tapes	12
h_{SC} (μm)	Thickness of HTS Tapes	100
D (mm)	Rotor winding average diameter	2738
L (mm)	Effective length of Generator	1682
N	Number of Turns in Each Coil	196
d (mm)	Distance between coils	10
J_{c0} (A/m^2)	Critical current density at 77 K $I_c/(w_{SC}\ h_{SC})$	2.5×10^{10}
σ_b (S/m)	Permeability of the cavity	1
τ (s)	Current increase and decrease rate	20
E_c (V/m)	Characteristic electric field	1×10^{-4}
n	Non-linear $E - J$ relation exponent	22
B_0 (T)	Critical current density parameter parametresiParameter of the critical current density	0.36
β	Critical current density parameter	1.2
α	Critical current density parameter	1

We began our analysis by examining the thermal behavior of the coil system with no liquid nitrogen flow (v_x=0, v_y=0). According to our simulation results, the system can withstand approximately 14 s of current increase before entering a "quench" state, where the temperature surpasses the critical transition temperature of 88 K for superconducting tapes. This quenching process initiates at the top left corner of the uppermost coil in the stack of 10 coils and then propagates throughout the entire system.

Upon the introduction of liquid nitrogen flow, we observed extended quench times of approximately 22 s and 46 s for flow rates of v_x=2 m/s, v_y=2 m/s and v_x=4 m/s, v_y=4 m/s respectively. These values are significant when compared to the 14 s quench time at zero flow, highlighting the efficacy of liquid nitrogen in delaying quench initiation. The numerical analysis results show that the presence of liquid nitrogen modifies the thermal environment of the coils. Specifically, the temperature rise observed in Fig. 2 follows a quadratic trend, meaning the temperature increases at a rate proportional to the square of the time. This behavior is less pronounced with the liquid nitrogen flow, demonstrating its cooling effect. Quantitatively, without liquid nitrogen flow, the system reaches a quench state rapidly, within 14 s. However, with liquid nitrogen cooling at v_x=2 m/s and v_y=2 m/s the quench time is extended to 22 s. At a higher flow rate of v_x=4 m/s and v_y=4 m/s, the quench time further extends to 46 s. These extended times indicate that the cooling provided by liquid nitrogen significantly reduces the rate of temperature increase, delaying the onset of quenching.

These deviations can be ascribed to a localized thermal runaway near the quench transition, where the heat generated from AC losses exceeds the cooling effect of liquid nitrogen, resulting in the temperature spike observed [39]. As the system approaches the quenching condition, the temperature distribution becomes increasingly uneven due to the current sharing transition between the superconducting and normal state regions of the HTS tape. This transition is influenced by external magnetic fields and current density, which may lead to the anomalies detected.

Additionally, the observed temperature increase within the coils, even with the liquid nitrogen flow, indicates that heat flux is concentrated in specific areas. This concentration of heat may be due to the geometric arrangement of the coils or the distribution of the electromagnetic field, which affects the local cooling effectiveness. These findings are particularly relevant to superconducting generators, as uneven temperature distribution can lead to thermal hotspots, reducing the overall efficiency and reliability of the system. Future improvements in the cooling system design and the layout of HTS tapes should address these issues to mitigate thermal risks and ensure uniform temperature management across the entire superconducting generator. By optimizing these aspects, it will be possible to enhance the performance and durability of superconducting generators.

In our exploration of the thermal dynamics within the rotor coil

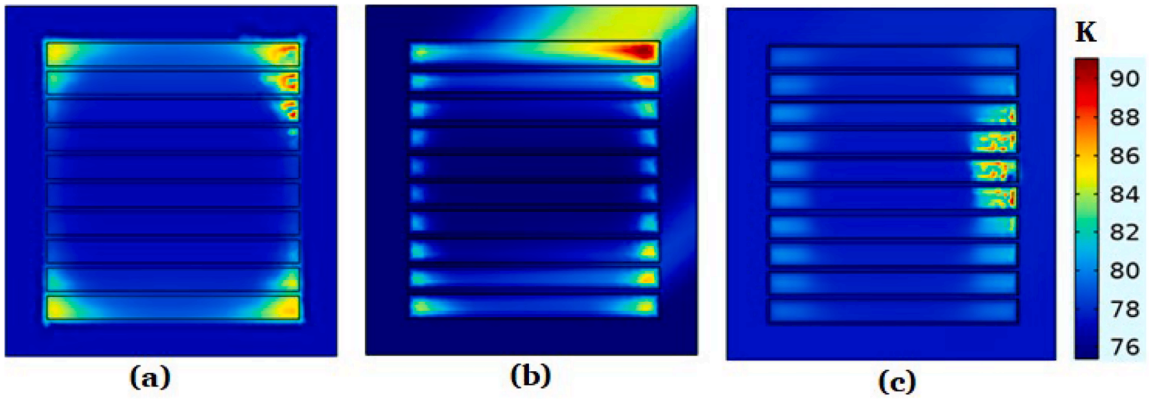

Fig. 2. Heat dissipation in rotor coils: Temperature distribution over the superconducting coils for (v_x, v_y, t) of (a) (0, 0, 14 s), (b) (2 m/s, 2 m/s, 22 s), and (c) (4 m/s, 4 m/s, 46 s).

systems of a 10 MW superconducting generator, we have placed particular emphasis on understanding the interaction between magnetic field distribution and coil temperature profiles. Through our foundational modeling, we have simulated the conditions wherein magnetic field lines deviate from the ideal axial orientation, particularly around the edge coils. This deviation is visually represented in Fig. 3, which showcases the magnetic field distribution around the superconducting racetrack-type "pancake" coil stacks placed within the *xy*-plane, with current flowing in the *z*-direction and liquid nitrogen flowing in the *xy*-direction for cooling.

The trajectory of the magnetic field lines near the edge coils, as depicted in Fig. 3, reveals a marked divergence from the axial orientation. This is particularly evident in coils No. 1 and No. 10, where the field lines show a concentrated deviation and a subsequent increase in the magnetic field's perpendicular component. This intensification leads to a reduction in the critical current density of these coils, as the superconducting material's ability to carry current without resistance is diminished in the presence of a stronger perpendicular magnetic field.

The impact of the increased perpendicular magnetic field component is further corroborated by temperature distribution analyses. The outermost coils (1 and 10) exhibit significant temperature changes due to the self-field effect of neighboring coils, leading to a higher rate of heat generation and a reduction in critical current density as the temperature rises. Fig. 4 provides a detailed view of this asymmetrical temperature distribution, which aligns with the alterations in the magnetic field observed in Fig. 3.

Moreover, our simulations have shown that the inner coils, particularly coils 5 and 6, experience initial heating when subjected to a

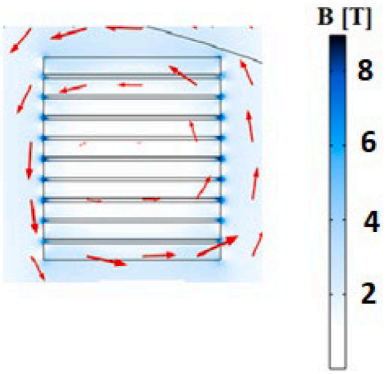

Fig. 3. Cross-sectional visualization of the magnetic field distribution in a stack of racetrack-type pancake coils used in a superconducting generator. The arrows indicate the direction of the magnetic field lines, with the color gradient representing the field intensity measured in teslas (T).

nitrogen flow velocity of 5.66 m/s (v_x=v_y=4.0 m/s). Specifically, the temperature on the surface of these coils rises from an initial value of 77 K to approximately 85 K within the first 10 s of operation. This initial heating can be quantitatively linked to the decrease in the critical current density as the temperature increases. The numerical results indicate that the critical current density decreases by approximately 15% for every 5 K rise in temperature. As the current magnitude increases, the temperature continues to rise, reaching a peak of 95 K at the 20-second mark, which leads to the formation of thermal zones at the ends of the inner coils. These thermal zones, initially confined to small areas, expand in width over time due to the continuous increase in temperature and the redistribution of the heat flux within the coils.

Our findings emphasize the necessity of a balanced cooling mechanism and the importance of considering both internal and external factors, such as neighboring coil self-fields and induced magnetization currents, which significantly influence temperature profiles across the coils. As shown in Fig. 6, the temperature distribution across the coils is heavily affected by these factors, leading to asymmetric heating patterns and localized hot spots. The critical current density maps in Fig. 7 further illustrate how the magnetic field distribution impacts thermal behavior, with regions of lower critical current density correlating with higher temperatures. This comprehensive understanding of the interplay between thermal and magnetic dynamics provides valuable insights into the design and operation of superconducting generators, highlighting the need for precise control of cooling mechanisms to ensure stable and efficient performance.

In our study, we closely examine the rate at which the electrical current increases and decreases, focusing on how these variations in current influence the overall performance and stability of the superconducting generator system, particularly in terms of electromagnetic and thermal responses. Fig. 4 presents the temperature distributions in the rotor coils at every 10 s assuming a time constant τ=20 s, which characterizes the period of current increase, for adopting velocity field v_x=v_y=5.0 m/s. Notably, the temperature remained stable throughout the system's current activation, without surpassing the superconductivity transition temperature. The highest temperature rise occurred in the top (10th) coil, peaking at approximately 77.6 K around t = 20 s. This can be attributed to the combined influence of self-fields from neighboring coils, which intensified the perpendicular component of the magnetic field penetrating the coil, thereby increasing current penetration.

As the order of the applied current increased, the heat generated in the inner coils was efficiently removed by the liquid nitrogen flow initially (t = 10 s). However, from t = 20 s onwards, thermal zones began forming at the ends of the inner coils, with their width expanding over time. This phenomenon may be linked to the decrease in the critical current density of the superconducting tapes as the temperature

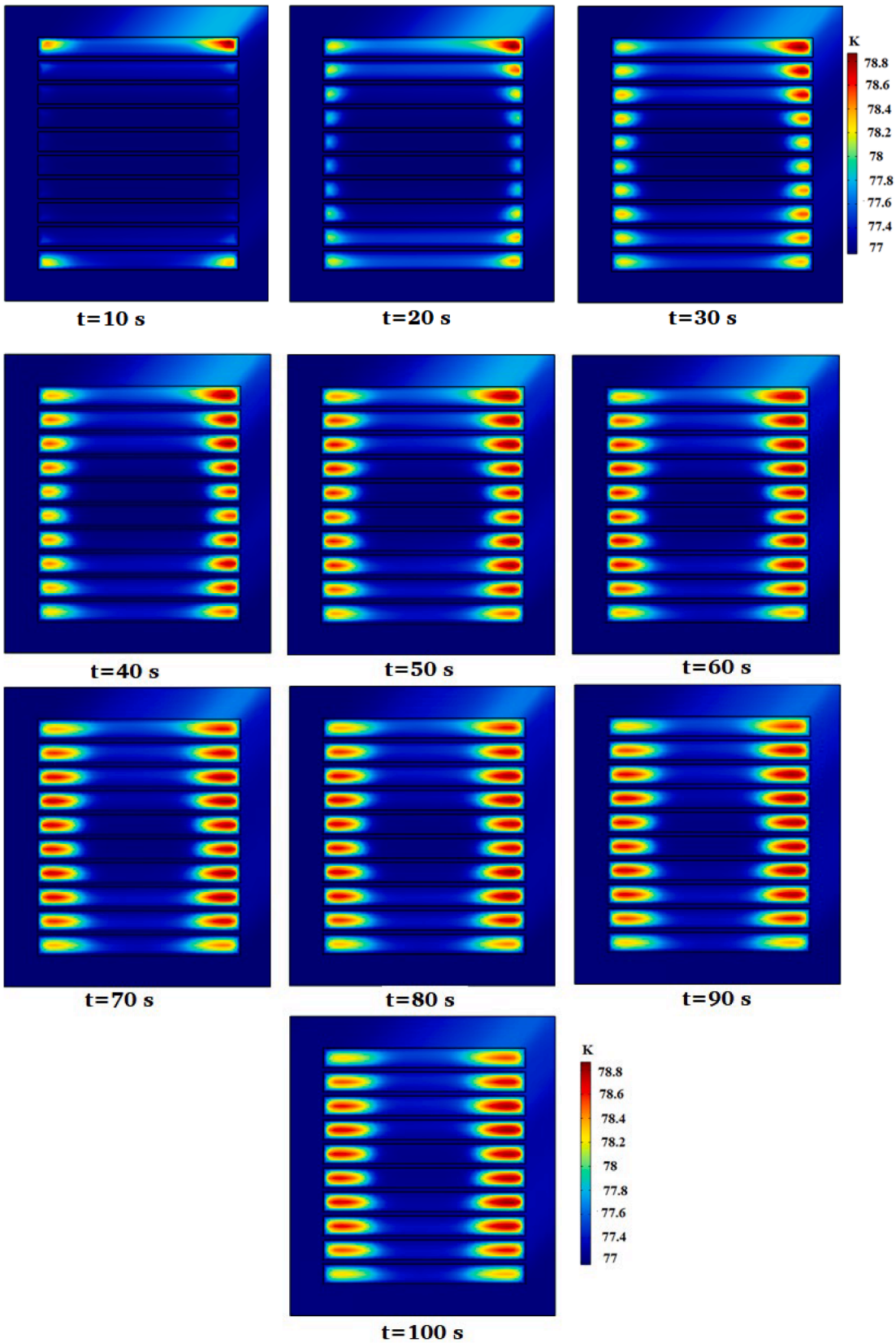

Fig. 4. Temperature distributions on the rotor coil cross section of the superconducting generator in 10 s intervals during each current increase.

increases. The analysis reveals that the critical current density decreases by approximately 15% for every 5 K rise in temperature. As the temperature of the coil surface rises from 77 K to 85 K within the first 10 s, and further to 95 K by the 20-second mark, the critical current density drops significantly. This reduction in critical current density results in localized heating and the formation of thermal zones at the ends of the inner coils, which expand over time due to the continued temperature increase and redistribution of heat flux within the coils. This detailed understanding underscores the direct relationship between temperature rise and the decrease in critical current density, explaining the observed thermal behavior in the superconducting coils.

In the outermost coils, the temperature on the coil surface increased with time as the current magnitude grew, eventually decreasing from $t =$ 60 s onwards. This behavior can be attributed to the rapid response of the outermost coils as the current approached the DC state.

We deduced that the outermost coils (1 and 10) show prominent temperature changes, predominantly due to the self-field of neighboring coils. Coils 5 and 6, being internal, manifest almost identical temperature profiles, hinting at the possible magnetic shielding from the external coils. The coils' centers experience less emphasized temperature variations than their edges.

The temperature distribution can be mathematically represented as:

$$T(r,t) = T_0 + \Delta T(r) \times F(t) \tag{15}$$

where $T(r,t)$ is the temperature at the point $r = \sqrt{x^2 + y^2}$ and time t, T_0 is the initial temperature, $\Delta T(r)$ is temperature change function at the point r. $F(t)$ in Eq. (15) is temporal variation function of temperature change and it represents how temperature changes over time. In this model, $\Delta T(r)$ captures how the temperature varies across different points in the coil, reflecting the influence of spatial factors such as proximity to other coils and magnetic shielding effects. $F(t)$ captures how the temperature changes over time due to factors like heat generation and dissipation. Separating these variables allows us to analyze and understand the effects of spatial distribution and time variation independently, which is useful for identifying the underlying causes of temperature changes and optimizing the thermal management of the superconducting coils.

Fig. 5 offers a more detailed view of the electro-thermal behavior of the outermost (10th) coil. The 1D plot of temperature change along the horizontal bisector of this coil reveals an asymmetrical temperature distribution. The temperature increase is higher at the end closer to the neighboring coils, potentially due to the self-field effect caused by these neighboring coils. Interestingly, the temperature in the coil first increased and then decreased as the current increased, suggesting a complex interplay of factors.

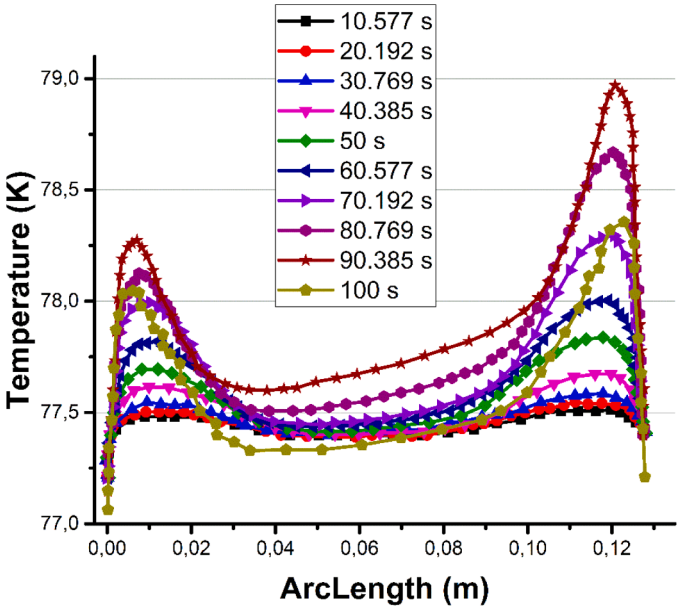

Fig. 5. Temperature distribution along the horizontal bisector of the top (10^{th}) coil in approximately 10 s intervals during the current increase when the time constant is τ=20 s.

Temperature variations within the coils were also linked to flux motion and current changes. At $t = 10$ s, the temperature rise was initially lower, as shown in Fig. 5, where the average coil temperature increased from 77 K to 77.5 K. However, by $t = 20$ s, the temperature increased more significantly to 78 K due to intensified flux motion. This increase in temperature is quantitatively linked to the critical current density reduction, which decreases by approximately 1.5% for every 0.5 K rise in temperature, as represented by the Eq. (13). As the temperature increased, the critical current density further decreased, resulting in diminished self-magnetic fields. The numerical analysis indicated that magnetic flux preferentially escaped from areas with lower critical current density, leading to a stronger decrease in the screening field in high-temperature regions [40]. This phenomenon is particularly evident when the self-magnetic field diminishes, causing magnetic flux to escape preferentially from areas with lower critical current density, as highlighted in the high-temperature regions. Furthermore, fluctuations in current at the ends of superconducting coils above the critical current could cause temperature instabilities, particularly in the end regions. This effect underscores the critical relationship between current fluctuations and temperature stability within the superconducting coils.

We compared the temperature distributions in the increasing and decreasing current cases in Figs. 4 and 6. For decreasing current, temperature differences in the outermost coil cross-section were observed to be 0.2 K higher than in the inner coils, primarily due to the higher self-field exposure of the outer coils. Notably, in the decreasing current case, temperature distributions appeared to be more homogeneous on the coil surfaces after $t = 60$ s, compared to the increasing current case. This behavior may be attributed to thermal losses caused by magnetization currents induced on the coil surfaces during current reduction, which were relatively higher than self-field losses. Overall, the temperature gradient between the center and edges of the coils was lower in the decreasing current case, and the calculated temperature was slightly lower than in the increasing current case.

From Fig. 6 we note that a more homogeneous temperature distribution is observed during the decreasing current scenario. The uniformity in this case might stem from the greater thermal losses induced by magnetization currents. This can be modeled by:

$$T(r,t) = T_{initial} - \Delta T'(r) \times F'(t) \tag{16}$$

Where ΔT'(r) represent the temperature function and ΔF'(t) time function during decreasing current conditions. In the same way, by separating the spatial distribution function $\Delta T'(r)$ and the time function $F'(t)$, one can independently analyze the effects of spatial and temporal factors on the temperature distribution. This separation simplifies the complex interaction between space and time, allowing us to model the thermal response more accurately under varying current conditions.

We further explored the effect of liquid nitrogen flow rates on temperature distribution in the coil system (Fig. 7). Our simulations revealed that, after a certain threshold of 5.0 m/s, the flow rate of liquid nitrogen had a limited impact on temperature distribution. Even for different flow rates up to 17.5 m/s, there were negligible differences in electrical behavior, especially under adiabatic conditions. Based on the results of our analysis, a liquid nitrogen velocity of v_x=10 m/s and v_y=10 m/s was found to be particularly effective in achieving stable temperature distribution, suggesting that this flow rate is appropriate for our system's cooling requirements. Although higher velocities did not significantly improve cooling efficiency, they also did not detrimentally affect the system. Therefore, while this velocity is not strictly "optimum"

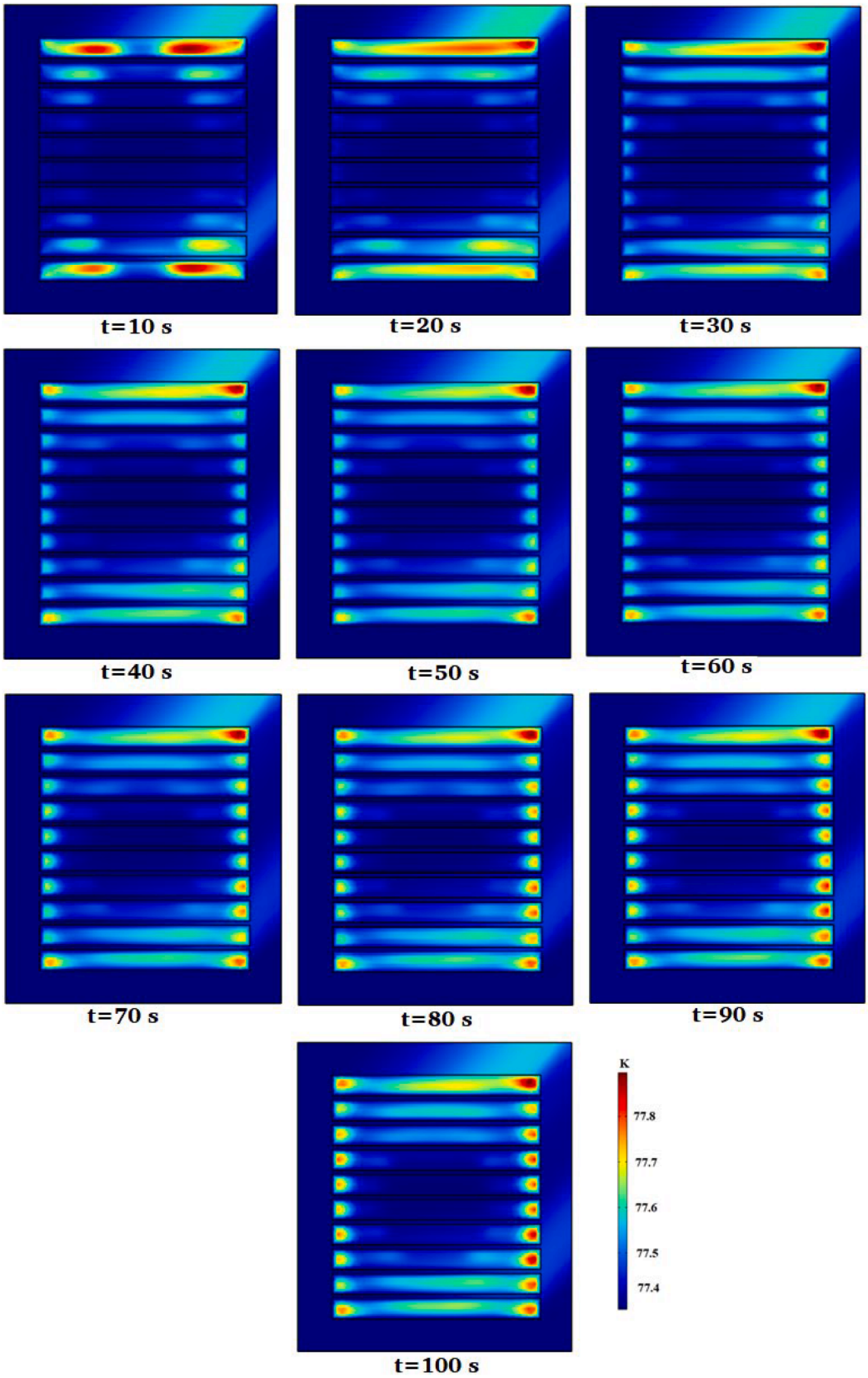

Fig. 6. Temperature distributions in superconducting rotor coils for decreasing current conditions for the same time constant (τ=20 s).

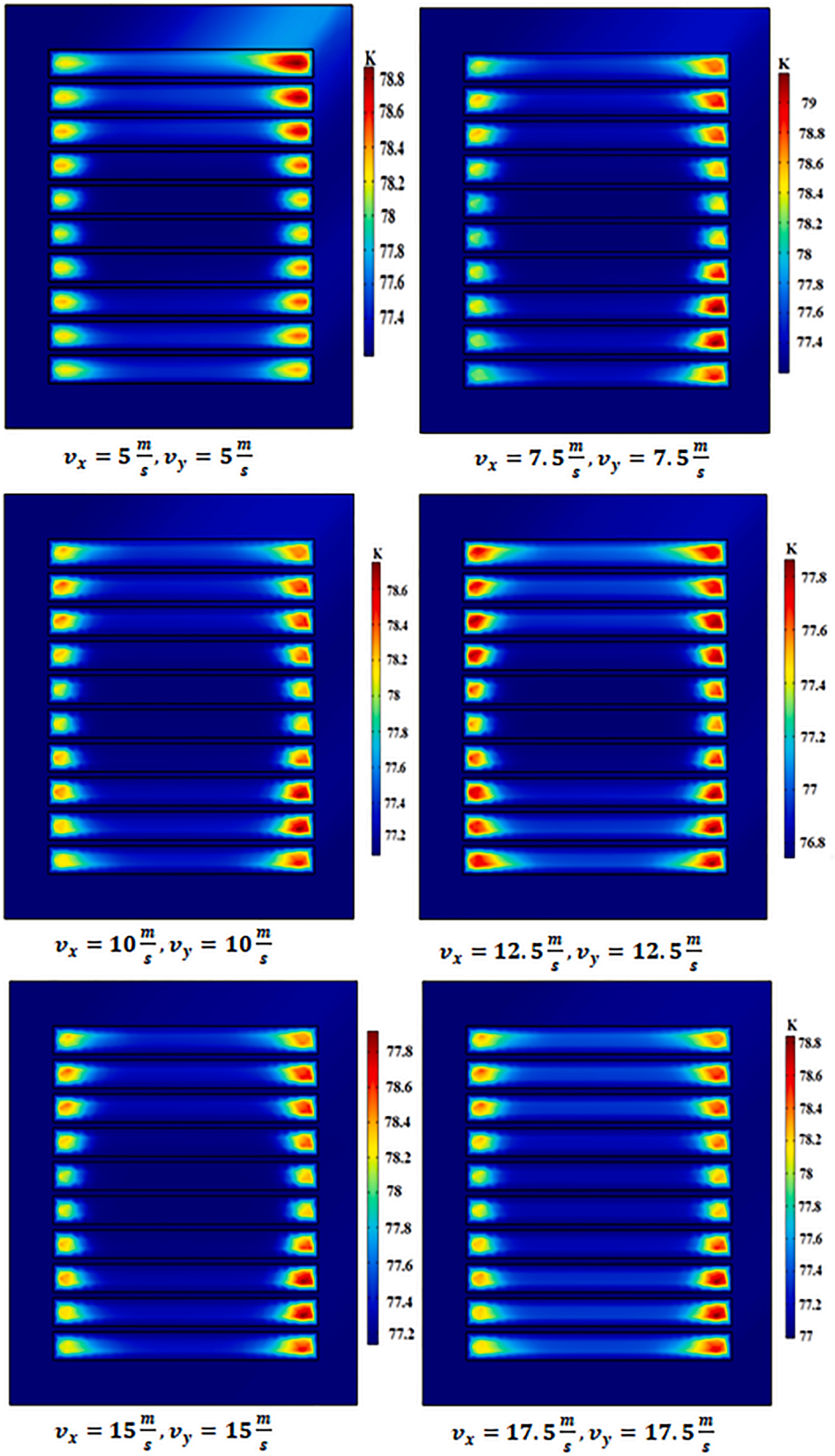

Fig. 7. Temperature distribution profiles in the superconducting rotor coil cross section at $t = 30$ s for different liquid nitrogen velocities (τ=20 s).

in a universal sense, it represents a practical and efficient choice based on the specific conditions and requirements of our coil system. The chosen velocity ensures adequate cooling while maintaining electrical and thermal stability, making it an appropriate selection from our range of considered conditions.

The introduction of a cooling mechanism such as liquid nitrogen introduces another layer of complexity to the model. The flow rate of liquid nitrogen, particularly after a certain threshold (5 m/s), seems to exhibit negligible effects on temperature distribution (as per Fig. 7). The cooling effect of liquid nitrogen is primarily due to its high heat capacity and low boiling point, allowing it to absorb significant amounts of heat from the superconducting coils. Initially, increasing the flow rate enhances cooling efficiency by increasing the rate of heat transfer from the coils to the coolant through rapid convection. However, beyond a certain threshold (approximately 5 m/s), the heat transfer process reaches a point where further increases in flow rate provide diminishing returns, as the heat transfer coefficient stabilizes and no longer significantly impacts the overall heat transfer rate. Additionally, the thermal resistance between the superconducting material and the liquid nitrogen means that once the flow is sufficient to overcome initial resistance, further increases do not substantially enhance cooling. This indicates that the system's temperature distribution becomes less sensitive to additional flow rate increases, highlighting the importance of identifying an optimal flow rate that maximizes cooling efficiency without unnecessary energy expenditure. This understanding is critical for designing efficient and cost-effective cooling systems for superconducting generators.

To incorporate this effect, the temperature function is augmented with a cooling term:

$$T(r,t) = T_0 + \Delta T(r) \times F(t) - C(v) \tag{17}$$

$C(v)$ in Eq. (17) is the cooling function based on the velocity v of liquid nitrogen. This cooling effect is assumed to be uniformly distributed throughout the coil system, hence it does not vary with r or t. The primary role of $C(v)$ is to account for the reduction in temperature due to the cooling capacity of the liquid nitrogen at a specific velocity. From Fig. 7, it is evident that the relationship between the flow rate and temperature, especially the nonlinear behaviors observed, can be captured by this cooling function in the following form:

$$T(r,t) = T_0 + \Delta T(r) \times F(t) - C(v) \tag{18}$$

where a and b are constants derived from fitting the data, v_{critical} is the critical velocity where temperature effects stabilize. The form of $C(v)$ as given in Eq. (18) is chosen based on the physical observation that the cooling effect increases with the flow rate but tends to plateau beyond a certain critical velocity (v_{critical}). The hyperbolic tangent function effectively models this behavior as it smoothly transitions from a linear increase to a plateau, representing the diminishing returns in cooling efficiency at higher velocities.

By fitting the data from Fig. 7, we can determine the constants a and b, which scale and shape the response curve, respectively. The parameter v_{critical} represents the velocity at which the cooling effect starts to level off, indicating the point beyond which further increases in flow rate do not significantly enhance cooling. This functional form captures the nonlinear relationship between the flow rate and temperature reduction, providing a clear and physically meaningful model for the cooling term $C(v)$.

In our model, $F(t)$ in Eqs. (15) and (17) is formulated to represent the time-dependent thermal dynamics within the superconducting coils. This function captures the transient thermal behaviors in response to electrical variations, reflecting how temperature changes over time due to factors such as current fluctuations and flux motion. The temperature distribution $T(r,t)$ is defined to map the spatial and temporal temperature variations across the coil, which is essential for assessing cooling efficiency and thermal responses under different operational conditions.

The temperature distribution correlates with the visual temperature profiles in figures like Fig. 4, depicting practical heating and cooling patterns observed in the system. The notation $F'(t)$, evolving into $\Delta F'(T)$, signifies the specific changes in the thermal profile, highlighting the complexity of cooling dynamics. These notations are used to indicate the progressive nature of thermal changes as the system evolves under operational conditions. The absence of direct plots of F or F' is due to our emphasis on integrated results like temperature distributions, which provide a more comprehensive understanding of thermal management in superconducting systems. By focusing on the combined spatial and temporal temperature distribution, we can offer a clearer picture of the overall thermal behavior, including the effectiveness of the cooling strategy and the system's response to varying electrical inputs. This integrated approach ensures that we capture the full scope of thermal dynamics, enabling more effective analysis and optimization of superconducting coil performance.

Fig. 8 illustrates the maximum temperature (T_{max}) values across the coil cross-section for various liquid nitrogen velocities during increasing current activation. Maximum temperatures increased with liquid nitrogen flow rates, but a saturation point was reached above a certain value. Beyond this saturation point, maximum temperatures fluctuated between 78.0 K and 79.5 K. The fluctuations observed around $t = 30$ s, when the current increase rate was highest, may be attributed to the delay in heat penetration compared to the magnetic field. The initial temperature starts at 77.5 K for the 5.0 m/s flow rate due to the reduced cooling efficiency at this lower velocity. In the simulation, the slower nitrogen flow leads to less effective heat removal before current activation, resulting in a slightly higher thermal equilibrium compared to higher flow rates.

The behavior of T_{max} shows a lowest value at 10 m/s, where cooling is most optimized, effectively balancing heat generation and dissipation. Conversely, T_{max} peaks at 7.5 m/s due to insufficient cooling during rapid heat generation, leading to localized temperature spikes. The irregular dependence of T_{max} on flow velocities arises from complex interactions in the simulation, such as fluid dynamics and coil geometry, which result in non-linear cooling efficiency.

The complex dependence on v_x and v_y can be attributed to several factors:

a) The fluctuations observed around $t = 30$ s, when the current increase rate was highest, may be due to the delay in heat penetration compared to the magnetic field. The thermal response of the coils takes time to adjust to the changes in current and magnetic fields, leading to these temperature oscillations.
b) As the liquid nitrogen velocity increases, the cooling efficiency improves, reducing the maximum temperature. However, after a certain point, the improvement in cooling becomes marginal, leading to a saturation effect. This is why the maximum temperatures do not significantly decrease beyond certain flow rates (e.g., v_x=v_y=15 m/s).
c) The coils may thermally be coupled, and the temperature distribution is influenced by the interactions between neighboring coils. The nonlinear behaviors observed in the plot, especially the peaks and troughs, result from these thermal interactions and the dynamic changes in current and magnetic fields.
d) The adiabatic conditions assumed in the analysis mean that heat is not exchanged with the surroundings, which can lead to more pronounced temperature fluctuations as the system tries to reach equilibrium.

Our cooling strategy analysis can be substantiated by the empirical approach detailed in Ref. [41]. This study demonstrates an effective rotating cryostat for isolating rotor components and employing a cryogenic cooling system directly integrated into the HTS coils. Their method of cooling HTS coils along with the rotor's metal parts provides enhanced thermal stability, especially in cryogenic supply system

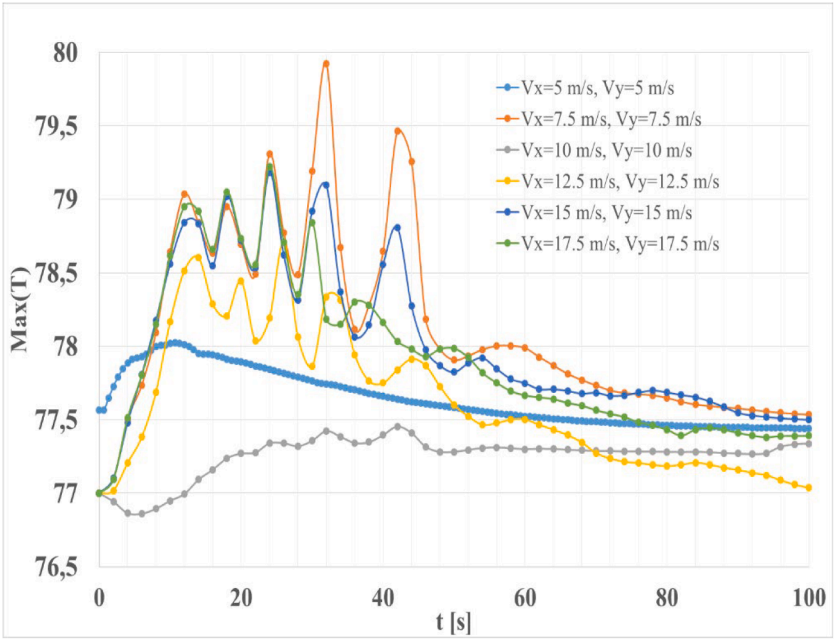

Fig. 8. Maximum temperature (T_{max} [K]) values in the coil cross-section during the field increase for different liquid nitrogen flow rates.

contingencies, aligning with our findings on the necessity of efficient cooling in superconducting generators. This parallel validates our simulation results and highlights the practicality of our proposed cooling techniques in real-world applications.

4. Conclusions

In conclusion, our research provides a detailed understanding of the thermal dynamics within the rotor coil systems for a 10 MW superconducting generator, particularly in relation to different cooling rates, current variations, and temperature distributions. Critical insights include:

a) Quench State Without Cooling: A superconducting system reaches a "quench" state when it loses its superconducting properties and transitions to a normal conductive state, resulting in a sudden increase in heat production. Without liquid nitrogen flow, the heat generated within the coils cannot be efficiently dissipated, causing the system to reach this quench state in approximately 14 s. This highlights the crucial importance of effective cooling mechanisms to maintain system stability and prevent thermal runaway.
b) Cooling Efficiency and Flow Rates: Liquid nitrogen flow removes heat from the superconducting coils. As the flow rate increases, the cooling efficiency improves because more heat is transferred away from the coils. However, beyond a certain threshold (e.g., 5 m/s), further increases in flow rate result in diminishing returns in cooling efficiency. This is because the system reaches a point where additional flow does not significantly enhance heat removal, indicating an optimal range for cooling performance.
c) Optimal Liquid Nitrogen Flow Rate: The identified optimal liquid nitrogen flow rate of v_x=v_y=10 m/s leverages effective cooling while avoiding rapid temperature fluctuations. At this flow rate, the system remains within safe temperature limits, balancing cooling efficiency and energy consumption. Higher flow rates do not substantially improve cooling performance and can lead to unnecessary energy use, making this rate the most practical for maintaining system stability.
d) Temperature Sensitivity: The temperature profiles across the coils are sensitive to both internal and external factors. Internal factors include the self-fields of neighboring coils, which can cause temperature variations due to their magnetic influence. External factors, such as induced magnetization currents, also affect temperature distribution. These factors create complex thermal dynamics that require careful consideration in system design to ensure uniform temperature management.
e) Mathematical Modeling: The mathematical models developed in this study accurately represent the temperature distribution and fluctuations within the coils. These models are valuable for predictive analyses, allowing for the simulation of thermal behavior under various operational conditions. By using these models, we can optimize the system's thermal management strategies, enhancing its performance and reliability.
f) Balanced Cooling Mechanism: Achieving a balanced cooling mechanism is crucial for the efficient operation of superconducting systems. Excessive cooling, indicated by higher flow rates of liquid nitrogen, can inadvertently lead to faster temperature rises due to the complex interactions between magnetic fields, flux motion, and critical current density. This emphasizes the need for a carefully calibrated cooling system that maintains thermal equilibrium without overcooling, which could destabilize the system.

These results provide a foundational understanding to improve the design and operation of superconducting generators. By tailoring cooling systems and understanding the behavior of these coils under various conditions, we can enhance the efficiency, longevity, and safety of these advanced energy systems. Future work could delve deeper into optimizing the cooling process and exploring the nuances of different superconducting materials. The findings from this study are significant, with implications extending beyond the realm of superconducting generators, potentially guiding advancements in related superconducting technologies.

CRediT authorship contribution statement

A. Erciyas: Writing – original draft, Software, Investigation, Data curation. **Ş. Yildiz:** Writing – review & editing, Supervision, Formal analysis. **F. Inanir:** Supervision, Software, Project administration, Formal analysis, Conceptualization.

Declaration of competing interest

The authors declare that they have no known competing financial interests or personal relationships that could have appeared to influence the work reported in this paper.

Data availability

Data will be made available on request.

References

[1] https://www.vestas.com/en/energy-solutions/offshore-wind-turbines/V236-15MW.

[2] A.B. Abrahamsen, B.B. Jensen, Superconducting direct drive wind turbine generators: advantages and challenges, in: S.M. Muyeen (Ed.), Wind Energy Conversion Systems: Technology and Trends, Springer, London, 2012, pp. 53–80, https://doi.org/10.1007/978-1-4471-2201-2_3.

[3] Y. Xu, L.-T. An, X.-P. Jia, B.-Z. Jia, N. Maki, Optimization study of the main parameters of different types of wind turbine generators, Supercond. Sci. Technol. 35 (3) (2022) 035007.

[4] S. Lengsfeld, J. Grundmann, M. Oomen, C. Vargas-Llanos, B. Ponick, M. Jung, Comparing armature windings for a 10 MW fully superconducting synchronous wind turbine generator, in: Proceedings of the 2022 12th International Conference on Power, Energy and Electrical Engineering (CPEEE 2022), Ritsumeikan Univ., Shiga, Japan, Feb. 25-27, 2022, pp. 49–53.

[5] X. Xu, Z. Huang, X. Huang, Z. Hong, Z. Jin, A method to predict AC loss on HTS Coils of a 30-kW generator using the T-A formulation, in: Physica C: Superconductivity and Its Applications, 591, 2021 1353973.

[6] G. Zhu, L. Li, X. Liu, H. Chen, W. Jiang, M. Xue, M. Li, Design optimization of a HTS-modulated PM wind generator, IEEE Trans. Appl. Superconduct. 31 (8) (2021) 5204004.

[7] C. Kim, H.J. Sung, B.S. Go, K. Sim, G.D. Nam, S. Kim, M. Park, Design, fabrication, and testing of a full-scale HTS coil for a 10 MW HTS wind power generator, IEEE Trans. Appl. Superconduct. 31 (5) (2021) 4900705. Art no.

[8] Y. Cheng, Y.Z. Zhang, R.H. Qu, D.W. Li, Y.Z. Liu, M. Noe, Design and analysis of 10 MW HTS double-stator flux-modulation generator for wind turbine, IEEE Trans. Appl. Superconduct. 31 (5) (2021) 5201408. Art no.

[9] M. Lee, M. Yoon, S.H. Park, W.S. Kim, J.K. Lee, K. Choi, Design of a 10 MVA fully HTS synchronous generator with dual field windings and 4 poles spanned armature windings, IEEE Trans. Appl. Superconduct. 31 (5) (2021) 5202605. Art no.

[10] C.C.T. Chow, M.D. Ainslie, K.T. Chau, High temperature superconducting rotating electrical machines: an overview, Energy Rep. 9 (2023) 1124–1156.

[11] T. Qu, Y. Li, P. Song, C. Hao, Q. Wu, C. Gu, J. Zhu, Z. Han, Design study of a 10-kW fully superconducting synchronous generator, IEEE Trans. Appl. Superconduct. 28 (4) (2018) 5207305. Art no.

[12] F. Inanir, A. Erciyas, R. Terzioglu, Design and AC loss analyze of a 10 MW-Rated HTS wind turbine generator, J. Supercond. Nov. Magn. 35 (11) (2022) 3189–3206.

[13] Y.F. Li, F. Feng, Y. Li, P. Song, S.N. Zou, M.S. Wu, C. Gu, P. Zeng, T.M. Qu, Numerical study on AC loss characteristics of ReBCO armature windings in a 15-kW class fully HTS generator, IEEE Trans. Appl. Superconduct. 27 (4) (2017) 5200206. Art no.

[14] M.M. Mussa, H.S. Noh, D. Kwon, Y. Ryu, Y.S. Choi, H. Lee, Thermal-quench behavior of non-insulated high-temperature superconducting (HTS) racetrack pancake coil with cooling channels through the epoxy surface, Results. Phys. 24 (2021) 104131.

[15] Y. Liu, et al., Investigation of ac loss of superconducting field coils in a double-stator superconducting flux modulation generator by using T-A formulation based finite element method, Supercond. Sci. Technol. 34 (2021) 055009.

[16] J. Sun, J. Zheng, Y. Song, L. Wang, X. Liu, X. Ni, Design of axial flux HTS machine prototype and AC losses calculation, IEEE Trans. Appl. Superconduct. 33 (8) (2023) 5203906.

[17] F. Weng, M. Zhang, A. Elwakeel, T. Lan, N. McNeill, W. Yuan, Transient test and AC loss study of a cryogenic propulsion unit for all electric aircraft, IEEe Access. 9 (2021) 59628–59636.

[18] Y. Zhang, Y. Cheng, R. Qu, D. Li, Y. Gao, Q. Wang, AC loss analysis and modular cryostat design of a 10-MW high-temperature superconducting double stator flux modulation machine, IEEe Trans. Ind. Appl. 58 (6) (2022) 7153.

[19] Y. Xu, N. Maki, M. Izumi, Study of key parameters and cryogenic vessel structure of 10-MW salient-pole wind turbine HTS generators, IEEE Trans. Appl. Superconduct. 25 (2) (2015) 5200406. Art no.

[20] Y. Choi, L. Dong, W. Dong, Optimal cool-down time of a 4 K superconducting magnet cooled by a two-stage cryocooler, Cryogenics. (Guildf) 52 (2012) 13–18.

[21] Y. Zhang, Y. Cheng, X. Fan, D. Li, R. Qu, Electromagnetic fault analysis of superconducting wind generator with different topologies, IEEe Trans. Appl. Supercond. 31 (5) (2021) 5202706. Art no.

[22] X. Zhu, M. Cheng, W. Hua, Z. Zhang, X. Ning, Thermal loss analysis, design, and test of a novel HTS magnet system for the double-stator field-modulation HTS electrical machine, IEEE Trans. Appl. Superconduct. 33 (6) (2023) 4901110. Art no.

[23] B. Shen, J. Li, J. Geng, L. Fu, X. Zhang, H. Zhang, C. Li, F. Grilli, T.A. Coombs, Investigation of AC losses in horizontally parallel HTS tapes, Supercond. Sci. Technol. 30 (7) (2017) 075006.

[24] Z.F. Chen, J.Y. Zhang, Z.Q. Wei, L.Z. Wang, Y. Xin, W.Z. Gong, H. Hong, Investigation of AC losses for HTS coils with parallel wound copper tapes, in: 2013 IEEE International Conference on Applied Superconductivity and Electromagnetic Devices (ASEMD), 2013, pp. 391–394.

[25] Y. Wang, X. Guan, J. Dai, Review of AC loss measuring methods for HTS tape and unit, IEEE Trans. Appl. Superconduct. 24 (5) (2014) 9002306.

[26] A.P. Malozemoff, G. Snitchler, Y. Mawatari, Tape-width dependence of AC losses in HTS cables, IEEE Trans. Appl. Superconduct. 19 (3) (2009) 3115–3118.

[27] E. Cuninkova, M. Pekarcikova, L. Frolek, S. Simon, M. Skarba, S. Hulacova, J. Krajcovic, Numerical and experimental design of the former for TORT cables, IEEE Trans. Appl. Superconduct. 33 (5) (2023) 4800805.

[28] L. Hao, J. Hu, H. Wei, Q. Wang, M. Tian, I. Patel, A. Shah, T. Coombs, Transport AC losses in multiple-layer roebel tapes, IEEE Trans. Appl. Superconduct. 33 (5) (2023) 4700805.

[29] D. Ruiz-Alonso, T. Coombs, A. Campbell, Computer modelling of high-temperature superconductors using an A–V formulation, Supercond. Sci. Technol. 17 (5) (2004) 305–310.

[30] Z. Hong, A.M. Campbell, T.A. Coombs, Numerical solution of critical state in superconductivity by finite element software, Supercond. Sci. Technol. 19 (12) (2006) 1246–1252.

[31] F. Inanir, R. Terzioglu, AC loss evaluation of a superconducting pancake coil with coated conductors using an extended A-V formulation, Physica C: Superconduct. Appl. 587 (2021) 1353910.

[32] A. Hennin, M. Lindmayer, M. Kurrat, Simulation setup for modeling the thermal, electric, and magnetic behavior of high temperature superconductors, Phys. Procedia 36 (2012) 1195–1205.

[33] M.D. Ainslie, H. Fujishiro, Modelling of bulk superconductor magnetization, Supercond. Sci. Technol. 28 (5) (2015) 53002, a.nd.

[34] M.D. Ainslie, Enhanced trapped field performance of bulk high-temperature superconductors using split coil, pulsed field magnetization with an iron yoke, Supercond. Sci. Technol. 29 (7) (2016) 74003, e.t al.:.

[35] J. Duron, F. Grilli, L. Antognazza, M. Decroux, B. Dutoit, Ø. Fischer, Finite-element modelling of YBCO fault current limiter with temperature dependent parameters, Supercond. Sci. Technol. 20 (4) (2007) 338–344.

[36] J. Ma, X. Li, J. Chen, Y. Li, Y. Zhao, A temperature-dependent multilayer model for direct current carrying HTS coated-conductors under perpendicular AC magnetic field, Superconduct. Sci. Technol. 33 (4) (2020) 045007.

[37] F. Gömöry, M. Vojenčiak, E. Pardo, J. Šouc, Magnetic flux penetration and AC loss in a composite superconducting wire with ferromagnetic parts, Superconductor Science and Technology 22 (3) (2009) 034017, https://doi.org/10.1088/0953-2048/22/3/034017.

[38] W.K. Chan, P.J. Masson, C.A. Luongo, J. Schwartz, Influence of inter-layer contact resistances on quench, propagation in YBa2Cu3Ox coated conductors, IEEe Trans. Appl. Supercond. 19 (2009) 2490–2495, a.nd.

[39] K. Hashimoto, H. Fujimaki, Thermal instability and flux motion in superconducting coils, IEEE Trans. Appl. Superconduct. 23 (3) (2013) 6600309.

[40] D.S. Dezhin, K.L. Kovalev, L.G. Verzhbitskiy, S.S. Kozub, V.P. Firsov, Design and testing of 200 kW synchronous motor with 2G HTS field coils, IOP Conf. Ser.: Earth Environ. Sci. 87 (3) (2017) 032007, https://doi.org/10.1088/1755-1315/87/3/032007.

[41] T. Dai, J. Li, Y. Tang, Y. Zhou, S. Chen, Y. Pan, Thermal analysis of a conduction-cooled HTS coil with heat disturbances, IEEE Trans. Appl. Superconduct. 15 (2) (2005) 1679–1682, https://doi.org/10.1109/TASC.2005.849231. June.